Prospects for the Observation of a Higgs Boson with $H \to \tau^+\tau^- \to l^+l^-\not{p}_t$ Associated with One Jet at the LHC

B. Mellado, W. Quayle, Sau Lan Wu

Physics Department
University of Wisconsin - Madison
Madison, Wisconsin 53706 USA

Abstract

The sensitivity of the LHC experiments to the Standard Model Higgs using $H \to \tau\tau \to l^+l^-\not{p}_t$ associated with one high P_T jet in the mass range $110 < M_H < 150\,\text{GeV/c}^2$ is investigated. A cut and Neural Network based event selections are chosen to optimize the expected signal significance with this decay mode. A signal significance of about $6.6\,\sigma$ can be achieved for $M_H = 120\,\text{GeV/c}^2$ with $30\,\text{fb}^{-1}$ of integrated luminosity for one experiment only. With this approach, experimental issues related to tagging forward jets and to the application of a central jet veto are simplified considerably.

1 Introduction

In the Standard Model (SM) of electro-weak and strong interactions, there are four types of gauge vector bosons (gluon, photon, W and Z) and twelve types of fermions (six quarks and six leptons) [1, 2, 3, 4]. These particles have been observed experimentally. At present, all the data obtained from the many experiments in particle physics are in agreement with the Standard Model. In the Standard Model, there is one particle, the Higgs boson, that is responsible for giving masses to all the particles [5, 6, 7, 8, 9, 10]. In this sense, the Higgs particle occupies a unique position.

Prior to the end of the year 2000, the Higgs particle was not observed experimentally. After the center-of-mass energy at the LEP accelerator of CERN reached $205\,\mathrm{GeV}$ in 2000, excess candidates began to show up in the Standard Model Higgs analysis in the ALEPH experiment, consistent with a Higgs mass, M_H, around $115\,\mathrm{GeV}/\mathrm{c}^2$ [11, 12].

One of the most exciting prospects for the LHC is confirming or rejecting the first possible experimental evidence for the Higgs particle at a mass around $115\,\mathrm{GeV}/\mathrm{c}^2$.

The Standard Model Higgs will be produced at the LHC via several mechanisms. The Higgs will be produced predominantly via gluon-gluon fusion [13] (see left diagram in Figure 1). For Higgs masses, such that $M_H > 100\,\mathrm{GeV}/\mathrm{c}^2$, the second dominant process is vector boson fusion (VBF) [14, 15] (see right diagram in Figure 1).
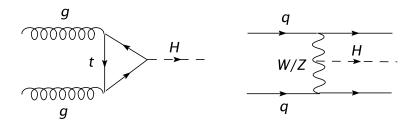

Figure 1: Leading Order diagrams of the dominant processes involving the production of Higgs at the LHC: Gluon-Gluon Fusion (left) and Vector Boson Fusion (right).

Even for these dominant processes, the Higgs production cross-section is small. Due to the large QCD backgrounds, identifying the Higgs requires rejecting backgrounds by several orders of magnitude. The identification of the Standard Model Higgs boson with a mass around $115\,\mathrm{GeV}/\mathrm{c}^2$ is especially challenging. Here, the most promising final states involve the Higgs decays $H \to \gamma\gamma$ [16, 17, 18] and $H \to \tau^+\tau^-$ [19, 20].

In the case of Gluon-Gluon Fusion, shown in Figure 1, the Higgs can be produced alone. However, when one of the gluons or top quarks emits a gluon, the Higgs is produced with the gluon, which is seen in the detector as a hadronic jet. When the Higgs has a significant transverse momentum the associated jet tends to be back-to-back with the Higgs in the transverse plane (for reasons of transverse momentum balance). In the case of Vector Boson Fusion, also shown in Figure 1, the Higgs is produced with

at least two jets. In both cases, jets produced in association with the Higgs are most useful in the identification of the Higgs, suppressing significantly the QCD background.

Early analyses performed at the parton level with the decays $H \to \tau^+\tau^- \to l^+l^-\not{p}_t$ associated with two high transverse momentum, P_T, jets indicated that this final state can be a powerful observation mode for a Higgs mass around 115 GeV/c^2 [19, 20]. The ATLAS and CMS collaborations have performed feasibility studies for these decay modes including more detailed detector description and the implementation of initial state and final state parton showers, hadronization and multiple interactions, which has confirmed the strong potential of this final state [21, 22]. However, this approach is intimately dependent upon the ability of tagging forward jets and applying a stringent central jet veto. The application of these experimental criteria will require a level of knowledge of the detectors' response, which may not be attained during the early stages of data taking at the LHC.

In this work we have explored the prospects of observing the decays $H \to \tau^+\tau^- \to l^+l^-\not{p}_t$ associated with one high P_T jet in the final state (a different approach was assessed within the context of Higgs searches at the Tevatron [23]). We have demonstrated that this final state enhances the potential for observing the Higgs at the LHC. Additionally, with this approach, experimental issues related to tagging forward jets and to the application of a central jet veto are considerably simplified.

2   Signal and Background Processes

For simplicity, we have considered only the two main Higgs production mechanisms at the LHC. Table 1 shows the cross-sections for these processes estimated for a center-of-mass of 14 TeV, as a function of the Higgs mass, in the range $110 < M_H < 150$ GeV/c^2. Shown are the Next-to-Leading Order (NLO) cross-section for the gluon-gluon fusion mechanism (σ_{gg}^{NLO}), as calculated by MC@NLO [24, 25], and the Leading-Order (LO) cross-section for the VBF mechanism (σ_{VBF}^{LO}), as calculated with PYTHIA6.2 [26, 27]. The proton structure function parametrization CTEQ was used to evaluate the proton-proton cross-sections [28]. Table 1 also displays the Higgs branching ratio into a τ pair, $\mathcal{B}(H \to \tau^+\tau^-)$, as calculated with the HDECAY package [29].

The basic experimental signature of interest consists of:

- Two oppositely charged leptons (electron or muon) with large transverse momentum.

- Large missing momentum, $\not{p}_t$, due to the presence of neutrinos in the final state.

- A large transverse momentum jet (tag jet).

Two relevant SM background processes are considered, which contribute to the final state specified above.

$M_H(\text{GeV}/c^2)$	σ_{gg}^{NLO} (pb)	σ_{VBF}^{LO} (pb)	$\mathcal{B}(H \to \tau^+\tau^-)$
110	36.64	4.65	0.0765
120	31.33	4.30	0.0685
130	27.09	3.99	0.0539
140	23.62	3.68	0.0355
150	20.77	3.38	0.0183

Table 1: Cross-sections for $pp \to H + X$ for different Higgs masses. Values of the Next-to-Leading Order cross-section for the gluon-gluon fusion mechanism, σ_{gg}^{NLO} and the Leading Order cross-section for the VBF mechanism, σ_{VBF}^{LO}, are given. The Higgs branching ratio into a τ pairs, $\mathcal{B}(H \to \tau^+\tau^-)$, is given in the last column.

- $pp \to Z/\gamma^* + X$ production with $Z/\gamma^* \to e^+e^-, \mu^+\mu^-, \tau^+\tau^-$ and $\tau \to l\nu_l\nu_\tau$. After requiring the presence of two charged leptons and large missing transverse momentum, $pp \to Z/\gamma^* + X$ with $Z/\gamma^* \to \tau^+\tau^- \to l^+l^-\displaystyle{\not}p_t$ process is expected to be the dominant background. The inclusive NLO cross-section of this process at the LHC yields 137 pb. A strong suppression factor can be achieved with the application of a dedicated event selection (see Sections 4 and 5).

- $pp \to t\bar{t}+X$ production with $t \to Wb$, and $W \to e\nu_e, \mu\nu_\mu, \tau\nu_\tau$ with $\tau \to l\nu_l\nu_\tau$. The NLO cross-section at the LHC yields 35.8 pb. This process is expected to display relatively large associated jet multiplicity, hence, the rejection of this background process is smaller with respect to that achieved for the $pp \to Z\gamma^* + X$ process (see Sections 4 and 5).

The contribution from events with at least one fake lepton in the final state is neglected here, due to the large fake lepton rejection expected to be attained with the CMS and ATLAS detectors.

3 MC Generation

Events corresponding to the signal process with the VBF mechanism have been generated with the LO matrix element based generator provided by PYTHIA6.2. The rest of the processes under consideration (Higgs via Gluon-Gluon Fusion and the background processes pointed in Section 2) have been treated with MC@NLO, which implements NLO matrix elements consistently matched with a parton shower generator. In order to assess the impact on the production of Z associated with hard jets coming from diagrams with weak bosons in the internal lines, the MadGraphII package was used [30, 31]. This program incorporates tree-level matrix elements for the process $pp \to Zjj$.

Higher order QCD corrections as well as effects due to off-shell tops have not been addressed here. These will be considered by the authors in future updates.

The impact of initial and final state QCD radiation, hadronization, multiple interactions and underlying event were simulated with PYTHIA6.2 and HERWIG6.5 [32, 33, 34], depending on the process. These MC programs were interfaced with the package ATLFAST in order to simulate the response of the ATLAS detector [35].

4   Event Selection

The following pre-selection cuts have been applied:

a. Require two high P_T leptons in the central region of the detector ($|\eta| < 2.5$). Due to trigger requirements, an event is accepted if at least one μ (e) has $P_T > 20\,\mathrm{GeV}$ ($P_T > 25\,\mathrm{GeV}$) or if at least two leptons are found with $P_T > 10\,\mathrm{GeV}$ for muons and $P_T > 15\,\mathrm{GeV}$ for electrons. An average 90% lepton identification efficiency is assumed. At this stage, a central b-jet veto is applied in order to suppress the contribution from $pp \to t\bar{t} + X$. Events are vetoed if a jet consistent with a b-jet hypothesis is found in the central region of the detector. An average 60% b-jet tagging efficiency is assumed in this region of the detector with rejections against c-jets and light jets of 10 and 100, respectively.

b. To suppress the contribution from $pp \to Z/\gamma^* + X$ with $Z/\gamma^* \to e^+e^-, \mu^+\mu^-$ and to further suppress $pp \to t\bar{t} + X$ production a cut on the invariant mass of the leptons is applied, $M_{ll} < 75\,\mathrm{GeV}$.

c. In order to reconstruct the mass of the Higgs candidate, it is assumed that the decay products of the τ's are collinear to the τ's themselves in the laboratory system [36] (usually referred to as the collinear approximation). The variables $x_{\tau 1}$ and $x_{\tau 2}$ are defined as the energy fraction of the decaying τ's carried by the charged leptons. By using the conservation of the transverse momentum, $\sum_{i=1,2} P_{T\tau i} = \sum_{i=1,2} P_{Tli} + \not{p}_T$. The variables $x_{\tau 1}$ and $x_{\tau 2}$ are the solution of two linear equations. The mass of the $\tau^+\tau^-$ pair, $M_{\tau\tau}$, can be computed as $M_{\tau\tau} = M_{ll}/\sqrt{x_{\tau 1}x_{\tau 2}}$. It is required that $0 < x_{\tau 1}, x_{\tau 2} < 1$.

d. The presence of at least one hadronic jet with $P_T > 30\,\mathrm{GeV}$ and $|\eta| < 4.9$ is required.

The discriminating power of various observables was examined after the application of cuts **a-d**. This exercise was performed for $M_H = 120\,\mathrm{GeV/c^2}$. In order to avoid biasses, an additional cut on the invariant mass of the Higgs candidate is applied, $110 < M_{\tau\tau} < 150\,\mathrm{GeV}$.[1] At this stage, the background is largely dominated by $pp \to Z/\gamma^* + X$ production (See Table 2 in Section 5). Figures 2 and 3 illustrate qualitative

---

[1]This cut is removed in the final evaluation of the signal significance. The signal significance is calculated using a likelihood technique, for which such a requirement is no longer necessary.
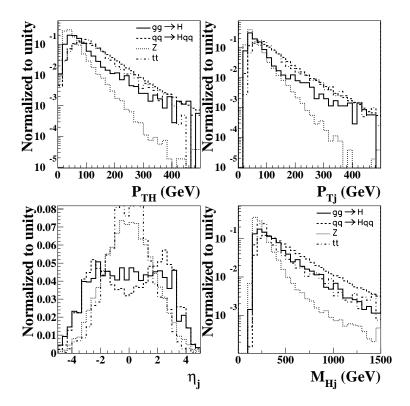
Figure 2: Signal and background kinematic distributions after the application of cuts **a-d** (see Section 4). An additional cut on the invariant mass of the τ pair, $110 < M_{\tau\tau} < 150\,\text{GeV}$, was applied. The upper left and right plots display the P_T of the Higgs candidate and the leading jet, respectively. The lower left and right plots correspond to the pseudorapidity of the leading jet and the invariant mass of the leading jet and the Higgs candidate, respectively. The solid and dashed curves correspond to Higgs production. The dotted-dashed and dotted curves correspond to the two main backgrounds considered here (see Section 2). All curves were normalized to unity.

differences among processes considered here. The solid and dashed curves correspond to Higgs production via gluon-gluon fusion and VBF, respectively. The dotted-dashed and dotted curves correspond to the two main backgrounds considered here (see Section 2). All curves were normalized to unity in the ranges specified in the plots.

The upper left and right plots in Figure 2 display the P_T of the Higgs candidate, P_{TH}, and the leading jet, P_{TJ}, respectively. The distribution of P_{TH} in $pp \rightarrow Z/\gamma^* + X$ is significantly softer with respect to that of the other processes considered here. The lower left plot in Figure 2 corresponds to the pseudorapidity of the leading jet. Leading jets in background production tend to be significantly more central than in signal production. Large P_T Z/γ^* production is dominated by $qg \rightarrow qZ/\gamma^*$ processes, in which the quark in the final state tends to be produced centrally. Higher order QCD corrections in $pp \rightarrow t\bar{t} + X$ production also favor central gluon radiation. On the other
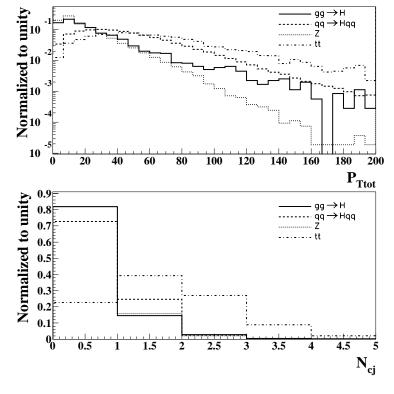
5

Figure 3: Signal and background kinematic distributions after the application of cuts **a-d** see Section 4). An additional cut on the invariant mass of the τ pair, $110 < M_{\tau\tau} < 150\,\mathrm{GeV}$, was applied. The upper plot shows the transverse momentum of the system made of the Higgs candidate and the leading jet. The lower plot corresponds to the number of sub-leading central jets (see Section 4). The solid and dashed curves correspond to Higgs production. The dotted-dashed and dotted curves correspond to the two main backgrounds considered here (see Section 2). All curves were normalized to unity.

hand, large transverse momentum production of Higgs via gluon-gluon fusion is mostly due to initial state radiation off incoming gluons, which favors the production of more forward jets. Finally, VBF represents the t-channel exchange of two weak bosons by two quarks, which favors the production of forward and very forward jets.

The lower plot in the right in Figure 2 displays the invariant mass of the Higgs candidate and the leading jet in the event, M_{HJ}. This variable is crucial to suppress $pp \to Z/\gamma^* + X$ production. This variable, however, fails to efficiently suppress $pp \to t\bar{t} + X$ production. Fortunately, the large jet multiplicity in $pp \to t\bar{t} + X$ production not associated to the actual top decay can be used to further suppress this background process. The upper plot in Figure 3 shows the P_T of the system made up by the Higgs candidate and the leading jet in the event. The lower plot in Figure 3 displays the number of sub-leading jets with $P_T > 30\,\mathrm{GeV}$ and $|\eta| < 2$, showing a qualitatively

6

different behavior in $pp \rightarrow t\bar{t} + X$ production. The application of a veto on central sub-leading jets is very efficient in further suppressing this background. It is worth noting that the probability for $pp \rightarrow t\bar{t} + X$ events to survive a veto on central jets does not depend strongly on the transverse momentum cut applied on these jets.

The following additional cuts are added to the event selection:

  e. Tagging jet is defined as the leading jet in the event. It is required that the tagging jet not be very central, $|\eta| > 1$. Events are vetoed in which at least one additional jet with $P_T > 30\,\text{GeV}$ and $|\eta| < 2$ is reconstructed.

  f. Tight cut on the Higgs candidate transverse momentum, $P_{TH} > 100\,\text{GeV}$.

  g. Tight cut on the invariant mass of the Higgs candidate and the tagging jet, $M_{HJ} > 700\,\text{GeV}$.

The event selection suggested in [19, 20] involves identifying events with two jets well separated in pseudorapidity. By requiring this, the signal contribution is dominated by Higgs production via VBF, in which, at least one of the jets is a very forward one. Additionally, the authors of [19, 20] envision the application of a stringent veto on events with central jets with $P_T > 20\,\text{GeV}$. The present event selection entails a number of crucial advantages over the the event selection suggested in [19, 20].

  1. As illustrated in the lower left plot in Figure 2, the bulk of the events display a tagging jet with $|\eta| < 4$. Therefore, in this approach there is no need to deal with very forward jets, which are challenging to identify and calibrate at the LHC. Moreover, the present event selection entails the presence of a very large P_T jets, which identification and calibration is significantly easier.

  2. Because the suppression of the $pp \rightarrow Z/\gamma^* + X$ relies on a tight cut on M_{HJ} as opposed to a stringent central jet veto, the requirements on sub-leading central jets are substantially looser. This renders the analysis more robust against the presence of additional jets produced by the underlying event and pile-up.

  3. Because of the requirement $P_{TH} > 100\,\text{GeV}$ and the presence of a very large P_T jet, the invariant mass resolution improves by 30% with respect to that obtained with the event selection suggested in [19, 20]. This is mainly due to the improvement in the resolution in the missing transverse momentum.

5 Results and Conclusions

Table 2 gives the effective cross-sections after the application of successive cuts in the event selection outlined in Section 4. Results are given in fb for the signal processes

7

Cut	$gg \to H$	VBF H	$pp \to Z/\gamma^* + X$			$pp \to t\bar{t} + X$
a	74.40	11.04	10.44×10^3	10.44×10^5	43.22	5.60×10^3
b	67.20	10.22	10.32×10^3	10.39×10^4	41.84	1760
c	47.3	8.91	5690	2.34×10^4	32.13	350
d	26.51	8.57	1870	2440	31.40	347
e	16.73	4.93	1030	1370	12.21	46.43
f	1.72	2.05	81.6	25.2	3.38	16.66
g	0.43	0.76	3.22	0.60	1.11	5.48
	0.32	0.59	0.38	0	0.11	0.41

Table 2: Effective cross-sections (in fb) for signal ($M_H = 120 \, \text{GeV}/c^2$) and background processes after the applications of cuts **a-g** specified in Section 4. The effective cross-sections in a mass window $110 < M_{\tau\tau} < 150 \, \text{GeV}$ are reported in the last row. The three columns for the process $pp \to Z/\gamma^* + X$, correspond to the contribution from QCD $Z/\gamma^* \to \tau^+\tau^-$, $Z/\gamma^* \to e^+e^-, \mu^+\mu^-$ and Electro-Weak $pp \to Zjj$ production, respectively.

with $M_H = 120$ and the two major background processes considered here. Results are also given after the application of a mass window $110 < M_{\tau\tau} < 150 \, \text{GeV}$. An excellent signal-to-background ratio of about 1 can be achieved. This is further illustrated in Figure 4, which displays the distribution of $M_{\tau\tau}$ (in fb/7 GeV) after the application of cuts **a-g** given in Section 4. The solid line corresponds to the total contribution of signal and background processes. The dotted and dotted-dashed lines correspond to the total background contribution and the contribution from $pp \to t\bar{t} + X$ alone, respectively. The contribution from $pp \to Z/\gamma^* + X$ with $Z/\gamma^* \to e^+e^-, \mu^+\mu^-$ is negligible in the mass window. The contribution of $pp \to Zjj$ from diagrams with weak bosons in the internal lines contributed to about 20% of the effective cross-section for $pp \to Z/\gamma^* + X$ in the mass window.

Figure 4 illustrates the different shapes of the $M_{\tau\tau}$ distributions for the two major backgrounds. While the contribution from $pp \to t\bar{t}+X$ is relatively flat, the contribution from $pp \to Z/\gamma^* + X$ displays a steep behavior, which is a combination of resolution effects and the presence of large mass Z/γ^* production.

It is evident from Figure 4 that a good control of the shape of the $M_{\tau\tau}$ distribution is crucial for establishing a compelling deviation from a purely background hypothesis. For the purpose of detailed studies of background estimation, two different event selections with little overlap were defined to address the two main backgrounds. The background normalization and shape of the $M_{\tau\tau}$ can be studied in these control samples and then extrapolated to the region of the phase space under study, as suggested in [37]. It has been demonstrated that by means of an analysis based on LO Matrix Elements the normalization of top backgrounds in $H \to W^+W^- \to l^+l^- \slashed{p}_t$ searches at the LHC can be determined with an accuracy of better than 10% [37].
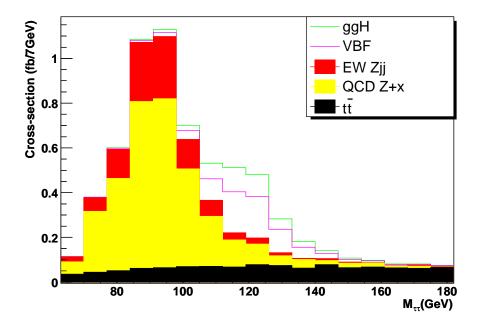
Figure 4: Distribution of $M_{\tau\tau}$ (in fb/7 GeV) after the application of cuts **a-g** given in Section 4. The solid line corresponds to the total contribution of signal and background processes. Histograms are staggered with the following order: $pp \rightarrow t\bar{t} + X$, $pp \rightarrow Z/\gamma^* + X$ (the contribution from Electro-weak Zjj is given by the dark histogram), VBF H and $gg \rightarrow H$.

The control sample to study $pp \rightarrow Z/\gamma^* + X$ includes all cuts presented in Section 4 except for requiring that the tagging jet be very central, $|\eta| < 1$, and a change in cut **g**, where $250 < M_{HJ} < 400$ GeV is used instead. As for the control sample to study $pp \rightarrow t\bar{t} + X$, the requirement of a b-jet veto is removed from cut **a**, in cut **e** the tagging jet is requited to be central, $|\eta| < 2.5$, and no veto on additional jets is applied. In addition, the transverse momentum of the system made by the Higgs candidate and the tagging jet is required to be larger than 100 GeV. Table 3 displays the contribution from signal and background processes after the application of these two event selections. Both event selections provide relatively clean environments to study the corresponding backgrounds. With $30 \, \mathrm{fb}^{-1}$ of integrated luminosity the background normalization will be understood to better than 10%.

The expected signal significance was calculated using a likelihood technique [38, 39]. Table 4 shows the expected signal significance as a function of the Higgs mass with $30 \, \mathrm{fb}^{-1}$ of integrated luminosity (for one experiment only). A 10% systematic error on the background estimation has been assumed.

Table 4 also reports the results obtained with a multivariate analysis performed with the help of Neural Network (NN) algorithms. For this purpose, NN's have been

9

Control Sample	$gg \to H$	VBF H	$pp \to Z/\gamma^* + X$	$pp \to t\bar{t} + X$
$pp \to Z/\gamma^* + X$	0.41	0.29	65.2	5.38
$pp \to t\bar{t} + X$	0.21	0.03	0.51	40.5

Table 3: Effective cross-sections (in fb) for signal ($M_H = 120\,\mathrm{GeV/c^2}$) and background processes after the applications of cuts for two control samples to study major backgrounds.

trained using the following discriminating variables: pseudorapidity of the tagging jet [2], M_{HJ} and P_{TH}. A net improvement in the signal significance of about 25% over the classical cut analysis can be achieved.

Higgs Mass (GeV/c^2)	110	120	130	140	150
Signal Significance for cut analysis (σ)	4.3	5.0	4.8	3.6	2.1
Signal Significance for NN analysis (σ)	5.5	6.6	6.3	4.8	2.8

Table 4: Expected signal significance for $H \to \tau^+\tau^- \to l^+l^- \not{p}_t$ associated with one high P_T jet as a function of the Higgs mass with $30\,\mathrm{fb^{-1}}$ of integrated luminosity (one experiment only). A 10% systematic error on the background estimation has been assumed. Results are given for the cut and NN based analyses.

The feasibility of searches for Minimal Super-Symmetric Higgs at the LHC with this final state needs to be investigated. It is worth noting that the approach presented in this work can be applied to other Higgs decays [40]. Generally speaking, this approach can be applied in searches of particles produced via the t-channel exchange of weak bosons.

6   Acknowledgments

---

[2] The requirement that $|\eta| < 1$ placed in cut **e** (see Section 4) was removed for the NN training.

References

[1] S. L. Glashow, Nucl. Phys. **B22** (1961) 579

[2] S. Weinberg, Phys. Rev. Lett. **19** (1967) 1264

[3] A. Salam, Proceedings to the Eigth Nobel Symposium, May 1968, ed: N. Svartholm (Wiley, 1968) 357

[4] S.L. Glashow, J. Iliopoulos and L. Maiani, Phys. Rev. **D2** (1970) 1285

[5] F. Englert, R. Brout, Phys. Rev. Lett. **13** (1964) 321

[6] P. W. Higgs, Phys. Lett. **12** (1964) 132

[7] P. W. Higgs, Phys. Rev. Lett. **13** (1964) 508

[8] P. W. Higgs, Phys. Rev. **145** (1966) 1156

[9] G. S. Guralnik, C.R. Hagen and T.W.B. Kibble, Phys. Rev. Lett. **13** (1964) 585

[10] T.W.B. Kibble, Phys. Rev. **155** (1967) 1554

[11] ALEPH Collaboration, R. Barate *et al.*, Phys. Lett. **B495** (2000) 1

[12] P. McNamara and Sau Lan Wu, Higgs Particle in the Standard Model: Experimental Results from LEP, Reports on Progress in Physics **65** (2002) 465

[13] H.M. Georgi, S.L. Glashow, M.E. Machacek and D.V. Nanopoulos, Phys. Rev. Lett. **40** (1978) 11

[14] R. Cahn and S. Dawson, Phys. Lett. **B136** (1984) 196

[15] G. Kane, W. Repko and W. Rolnick, Phys. Lett. **B148** (1984) 367

[16] CMS Collaboration, CMS ECAL Technical Design Report, CERN/LHCC 97-33

[17] ATLAS Collaboration, Detector and Physics Performance Technical Design Report, CERN-LHCC/99-14 (1999)

[18] S. Abdullin *et al.*, Phys. Lett. **B431** (1998) 410

[19] K. Hagiwara, D.L. Rainwater and D. Zeppenfeld, Phys. Rev. **D59** (1998) 014037

[20] T. Plehn, D.L. Rainwater and D. Zeppenfeld, Phys. Rev. **D61** (2000) 093005

[21] S. Adbullin *et al.*, Summary of the CMS Potential for the Higgs Boson Discovery, CMS NOTE 2003/033 (2003)

[22] S. Asai *et al.*, Search for the Standard Model Higgs Boson in ATLAS using Vector Boson Fusion, ATLAS Scientific Note SN-ATLAS-2003-024 (2003), submitted to EPJ, hep-ph/0402254

[23] A. Belyaev, T. Han and R. Rosenfeld, JHEP **0307** (2002) 021

[24] S. Frixione and B.R. Webber, JHEP **0206** (2002) 029

[25] S. Frixione and B.R. Webber, JHEP **0308** (2003) 007

[26] T. Sjöstrand, Comp. Phys. Comm. **82** (1994) 74

[27] T. Sjöstrand *et al.*, Comp. Phys. Comm. **135** (2000) 238

[28] H.L. Lai *et al.*, Eur. Phys. J. **C12** (2000) 375

[29] A. Djouadi, J. Kalinowski and M. Spira, HDECAY: a Program for Higgs Boson Decays in the Standard Model and its Supersymmetric Extention, Comp. Phys. Comm. **108** (1998) 56

[30] T. Stelzer and W.F. Long, Phys. Comm. **81** (1994) 357

[31] F. Maltoni and T. Stelzer, MadEvent: Automatic Event Generation with Mad-Graph, hep-ph/0208156 (2002)

[32] G. Marchesini and B.R. Webber, Nucl. Phys. **B310** (1988) 461

[33] G. Marchesini *et al.*, Comp. Phys. Comm. **67** (1992) 465

[34] G. Corcella *et al.*, JHEP **0101** (2001) 010

[35] E. Richter-Was, D. Froidevaux and L. Poggioli, ATLFAST2.0 a Fast Simulation Package for ATLAS, ATLAS Note ATL-PHYS-98-131 (1998)

[36] R. K. Ellis *et al.*, Nucl. Phys. **B297** (1988) 221

[37] N. Kauer, Top Background for $H \to WW$ searches at the LHC, hep-ph/0404045 (2004)

[38] K. Cranmer, B. Mellado, W. Quayle and Sau Lan Wu, Confidence Level Calculations in the Search for Higgs Bosons Decay $H \to W^+W^- \to l^+l^- \not{p}_T$ Using Vector Boson Fusion, ATLAS Note ATL-PHYS-2003-008 (2003)

[39] K. Cranmer, B. Mellado, W. Quayle and Sau Lan Wu, Challenges of Moving the LEP Higgs Statistics to the LHC, physics/0312050 (2003)

[40] B. Mellado, W. Quayle and Sau Lan Wu, Prospects for the Observation of a Higgs Boson with $H \to W^+W^- \to l^+l^- \not{p}_t$ Associated with One Jet at the LHC, in preparation.